Predictions and measurements of scattering and absorption over broad wavelength ranges in tissue phantoms

Judith R. Mourant, Tamika Fuselier, James Boyer, Tamara M. Johnson, and Irving J. Bigio

Predictions from Mie theory regarding the wavelength dependence of scattering in tissue from the near UV to the near IR are discussed and compared with experiments on tissue phantoms. For large fiber separations it is shown that rapid, simultaneous measurements of the elastic scatter signal for several fiber separations can yield the absorption coefficient and reduced scattering coefficient. With this information, the size of the scattering particles can be estimated, and this is done for Intralipid. Measurements made at smaller source detector separations support Mie theory calculations, demonstrating that the sensitivity of elastic scatter measurements to morphological features, such as scatterer size, is enhanced when the distance between the source and detector fibers is small. © 1997 Optical Society of America

1. Introduction and Background

Multiple-wavelength measurements of light transport in tissue can yield information about scattering and absorption properties that are pertinent to the physiological state of the tissue. The scattering properties of tissue are related to tissue morphology, and the absorption properties are related to the tissue biochemistry. Several chromophores in tissue have absorption bands in the near UV, visible, and near IR, including hemoglobin, nicotinamide adenine dinucleotide, melanin, and bilirubin. A variety of techniques are being developed to measure scattering properties of tissue and to detect and measure concentrations of chromophores.[1–6] Frequently these techniques are based on the diffusion approximation and are single-wavelength techniques, although a few researchers have made broader wavelength measurements.[3,7]

Measurement over a broad wavelength range offers potential advantages over single-wavelength measurements. When one is working in the diffusion approximation, where contributions to the signal that are due to scattering and absorption can be separated, expected advantages of broad wavelength measurements are: (1) measurements of concentrations of several absorbers can be performed simultaneously with improved accuracy, and (2) knowledge of the wavelength dependence of scattering will aid in the determination of structural features. In geometries where the diffusion approximation is not valid (e.g., small separations of the source and detector), a method of separating the contributions to the signal that are due to scattering and absorption has not yet been developed. Nonetheless, recent *in vivo* clinical studies involving a statistically significant number of measurements have demonstrated that the measurement of elastic scatter or fluorescence over broad wavelength ranges has the potential to distinguish cancerous and noncancerous tissue.[8–11] These results could be improved on with detailed answers to the following questions: (1) What is the sensitivity of the measurements to specific features of the tissue? (2) How can the measurement procedures and equipment be adjusted to enhance sensitivity to specific features? As an approach to addressing the above two questions, in this paper we examine the wavelength dependence of scattering by employing both Mie theory calculations and experimental measurements of polystyrene spheres.[12]

Although the exact nature of the scattering centers in tissue has not been determined, it is possible to

The authors are with the Bioscience and Biotechnology Group CST-4, MS E535, Los Alamos National Laboratory, Los Alamos, New Mexico 87545.

Received 6 October 1995; revised manuscript received 6 June 1996.

0003-6935/97/040949-09$10.00/0

place some limits on scatterer sizes and refractive indices. Scattering is expected to occur from cells, organelles, and proteins. Mammalian cells vary in size from approximately 3 to 20 μm in diameter.[13] Organelles such as mitochondria and nuclei have dimensions in the range ~1–5 μm. Subnuclear components such as nucleoli and regions of condensed and extended chromatin may have dimensions as large as 1 μm. Proteins typically have dimensions of the order of fractions of a micrometer. For example, a hemoglobin molecule is roughly 64 Å in diameter. Therefore it is expected that scattering centers can vary in size from very small particles such as proteins, which have dimensions measured in angstroms, to cells 20 μm in diameter. There is also a range of indices of refraction in tissue. Extracellular fluid has a real refractive index between 1.348 and 1.351.[14] Refractive indices of the cytoplasm and nucleus of Chinese hamster cells have been measured to be 1.3703 and 1.392, respectively.[15] Materials of higher index such as lipids (1.46)[16] and proteins (1.51)[17] are also present in tissue.

The tissue parameters that determine light transport are the boundary conditions and, depending on the measurement geometry, a subset of the following parameters: the inverse mean free path for scattering μ_s, the inverse mean free path for absorption μ_a, the probability distribution of scattering angles $P(\theta)$, and the reduced scattering coefficient μ_s'. When source-to-detector separations are large (such that the diffusion approximation is valid), only μ_s' and μ_a are needed to describe light transport. When source-to-detector separations are small, μ_s, $P(\theta)$, and μ_a can all be important factors determining light transport. In this paper we examine both regimes. In Section 2, the expected wavelength dependence of the reduced scattering coefficient in tissue as a function of particle size is discussed. In Subsections 3.A and 3.B broad wavelength measurements of absorption and scattering coefficients with a cw system are presented for Intralipid and suspensions of polystyrene spheres. Using the wavelength dependence of the measured reduced scattering coefficient, the size of the scattering particles in Intralipid is estimated. In Subsection 3.C measurements of polystyrene spheres at small fiber separations are presented.

2. Theoretical Predictions

If simplifying assumptions are made that the scattering centers in tissue are homogeneous dielectric spheres and that the electromagnetic field incident on each sphere is a plane wave, Mie theory can be used to predict the wavelength dependence of the scattering. For a sphere of radius r and index of refraction n_s in a medium with index n_m, scattering is determined by the size parameter[18] $x = 2\pi r n_m/\lambda$ and the ratio of indices of refraction $m = n_s/n_m$. Mie theory can be used to calculate $P(\theta)$ and the efficiency factors for scattering and absorption Q_S and Q_a, respectively.[19] The efficiency factors for individual scattering events are related to the macroscopic scattering coefficients μ_s, μ_s', and μ_a by the following:

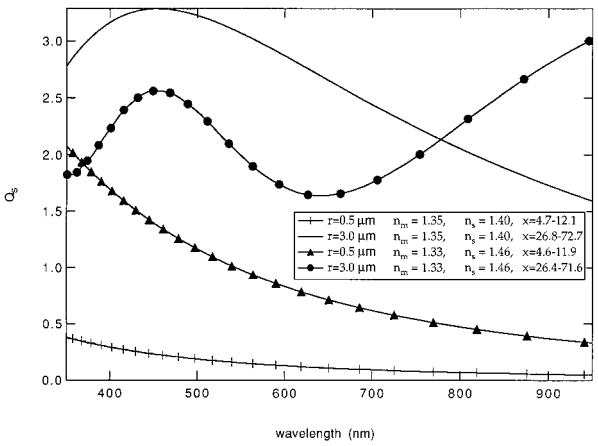

Fig. 1. Efficiency factor for scattering Q_s as a function of wavelength for 0.5- and 3.0-μm-radius spheres. Results are shown for both a sphere refractive index of 1.33 with a medium refractive index of 1.46 (m = 1.098) and for a sphere refractive index of 1.35 with a medium refractive index of 1.40 (m = 1.053).

$$\mu_s = Q_s N_s A_s, \tag{1}$$

$$\mu_{s'} = Q_s N_s A_s (1 - g), \tag{2}$$

$$\mu_a = Q_a N_s A_s. \tag{3}$$

N_s is the number density of spheres, $g = \langle \cos\theta \rangle$ is the expectation of the cosine of the photon scattering angle, and $A_s = \pi r^2$. For our calculations we assume that the light incident on the spheres is unpolarized.

Both Q_s and $P(\theta)$ are complicated and sometimes rapidly varying functions of wavelength. The wavelength dependence of Q_s, which is related to μ_s by Eq. (1), varies greatly with both the size and refractive index of the scatterer as demonstrated in Fig. 1. Figure 2 is a surface plot of $\log(P(\theta))$ for a wide range of wavelengths for a 0.5-μm sphere ($n_s = 1.46$ and $n_m = 1.33$). There are oscillations in $P(\theta)$ as a function of both wavelength and angle. Note that $P(180°)$ shows more structure as a function of wavelength than $P(0°)$. This structure depends on the scatterer.

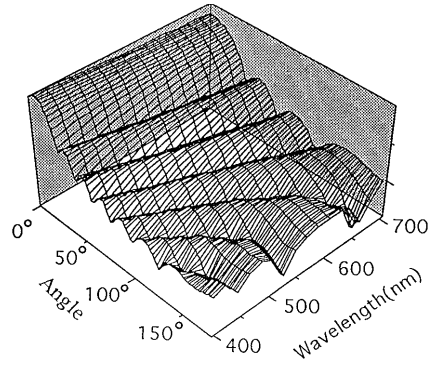

Fig. 2. $\mathrm{Log}(P(\theta))$ as a function of angle and wavelength for a 0.5-μm sphere. The index of the medium is taken to be 1.33 and the index of the sphere to be 1.46. (At a given wavelength $\int P(\theta) \sin\theta \, d\theta = 1$.)

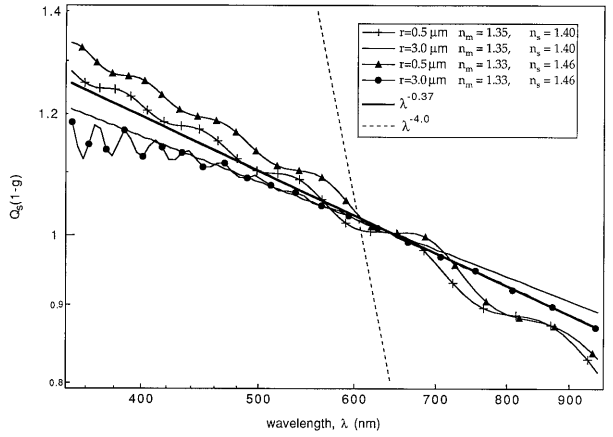

Fig. 3. Wavelength dependence of $Q_s(1 - g)$ for 0.5 and 3.0-μm-radius spheres. Results are shown for both $n_s = 1.46$ with $n_m = 1.33$ ($m = 1.1$, $x = 4.6$–10.5 for the 0.5-μm spheres and $x = 27.8$–62.7 for the 3.0-μm spheres) and for $n_s = 1.40$ with $n_m = 1.35$ ($m = 1.04$, $x = 4.7$–10.6 for the 0.5-μm spheres and $x = 28.3$–63.6 for the 3.0-μm spheres). The dashed line shows the λ^{-4} wavelength dependence of scatterers with a size parameter $x \ll 1$. (On a log-log plot a λ^{-n} dependence is a straight line.) Each curve has been multiplied by a constant to have a value of 1 at 600 nm.

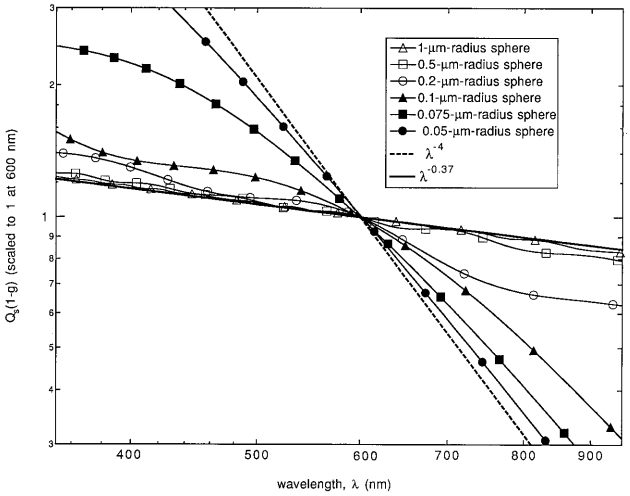

Fig. 4. Wavelength dependence of $Q_s(1 - g)$ for a wide range of sphere sizes. $n_s = 1.50$ and $n_m = 1.35$. All curves have been normalized to have a value of 1 at 600 nm. Deviations from a straight line indicate deviations from a λ^{-n} dependence.

Therefore measurements in geometries where sensitivity to high-angle scattering is enhanced are expected to be more useful for differentiating average structural features of the scatterers. Other authors have reached similar conclusions.[20,21]

Considering the complicated dependencies of both μ_s and $P(\theta)$ on wavelength one might expect $\mu_s' = \mu_s(1 - \langle \cos\theta \rangle)$ to be a rapidly varying function of wavelength. Although this is true for some values of x and m, for a wide range of size parameters and indices of refraction, μ_s' is a decreasing function of wavelength from 350 to 950 nm. For $1 < m < 1.1$ and $5 < x < 50$, $\mu_s' \propto \lambda^{-0.37}$ as shown by Graaff *et al.*[22] Figure 3 demonstrates that even for $4.6 < x < 65$, the relative amplitude of $Q_s(1 - g)$ varies from $\lambda^{-0.37}$ by less than 6% between 400 and 900 nm.

As the size parameter x decreases below 5, the wavelength dependence of $\mu_s'(\lambda)$ approaches the $1/\lambda^4$ dependence expected for Rayleigh scattering. This is demonstrated in Fig. 4. Although μ_s' can not be expressed accurately by the form λ^{-n} for all sphere sizes, there is a general trend that the wavelength dependence changes from λ^{-4} to $\lambda^{-0.37}$ as sphere size increases. All of the calculations shown in Fig. 4 were done with $m = 1.11$ ($n_s = 1.50$ and $n_m = 1.35$). Based on the indices of refraction of the biological components of tissue discussed above it is unlikely that m will be larger than this.

Smaller values of m have little effect on the wavelength dependence of μ_s' as shown in Fig. 5. Therefore the wavelength dependence of μ_s' can be used to estimate the size of the scatterers contributing to the elastic scatter signal without concern about the relative refractive indices of the scatterers. An example of this technique for estimating the size of the dominate scattering particle in Intralipid is given in Section 3.

3. Multiwavelength Measurements of Tissue Phantoms

A. Comparison of Theory and Experiment for Polystyrene Spheres

Measurements of polystyrene sphere suspensions were made to compare predicted and measured values of $\mu_s'(\lambda)$. The purpose of these measurements was to determine if the measured wavelength dependence of $\mu_s'(\lambda)$ agreed with predictions of Mie theory. The infinite diffusion theory approximation was used. The experimental system included uncooled CCD detectors and used one collection fiber that could be moved with respect to the delivery fiber [Fig. 6(b)]. A reference for the lamp was used to account accu-

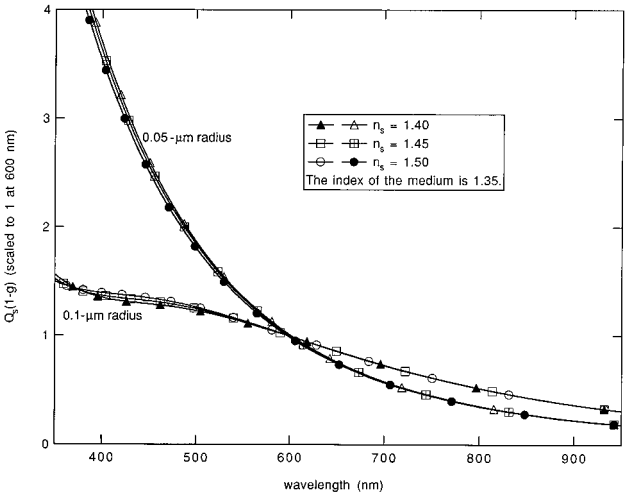

Fig. 5. Effect of changes in n_s on $Q_s(1 - g)$ for 0.05 and 0.1-μm-radius spheres. All curves have been normalized to have a value of 1 at 600 nm.

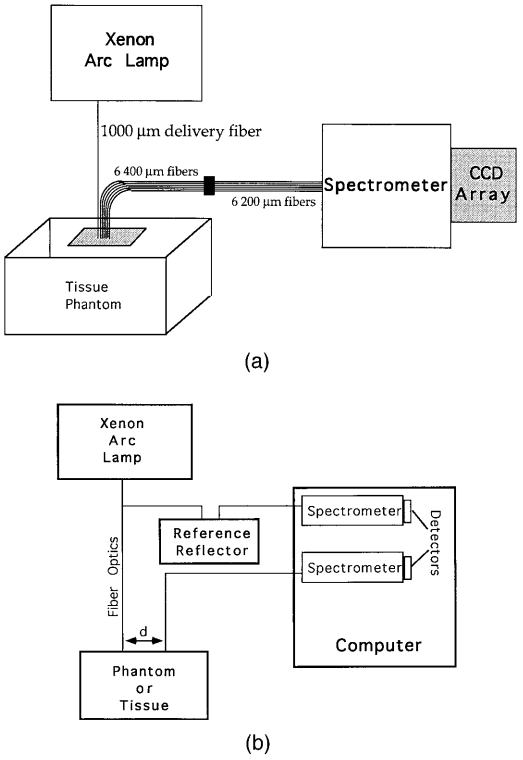

Fig. 6. Schematic of the instrumental systems. (a) The experimental system used for measurement of Intralipid. (b) The experimental system used for measurement of polystyrene spheres.

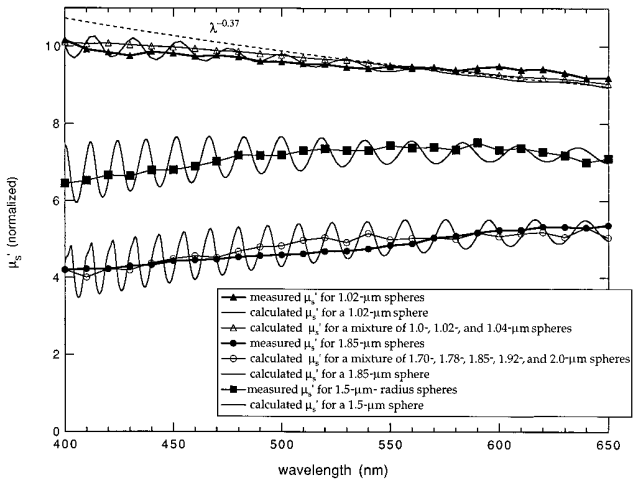

Fig. 7. Comparison of measured and calculated values of μ_s' for suspensions of 1.02-μm-, 1.5-μm-, and 1.85-μm-radius spheres. The curves have been scaled such that the area under the theoretical curves is equal to the area under the corresponding experimental curves.

rately for any changes in the lamp output during the course of the measurements.

The elastic scatter signals of aqueous suspensions of three sphere sizes were measured: 1.02 ± 0.02-μm-radius spheres, 1.5 ± 0.113-μm-radius spheres, and 1.85 ± 0.113-μm-radius spheres. The concentrations by weight of the spheres were, respectively, ~0.2% ($N_s = 4.18 \times 10^8/\text{cm}^3$), 0.5% ($N_s = 3.45 \times 10^{10}/\text{cm}^3$), and ~0.3% ($N_s = 1.08 \times 10^8/\text{cm}^3$). On a cubic grid, this gives shortest, nearest neighbor separations of 13.37, 3.07, and 21.0 μm, respectively.

A 400-μm optical fiber (0.22 NA) was used to deliver light to the sphere suspension, and a 600-μm optical fiber (0.48 NA) was used to collect light from the sphere suspension. The diffusion approximation was valid for the geometry employed in these measurements. The sample volume was a cylinder of depth ~6.5 cm and diameter ~7 cm. The fibers were placed approximately 3 cm into the suspensions of spheres. Measurements of the elastic scatter signal were made as a function of fiber separation for $d > 1$ cm.

Derivations of equations to determine μ_a and μ_s' from measurements of amplitude-modulated light transport in the diffusion approximation have been given by several authors and include the derivations for cw light.[23,24] These derivations rely on the fact that measurements of light intensity are made at multiple fiber separations, ρ. Expressions for $\mu_a(\lambda)$ and $\mu_s'(\lambda)$ are given in Eqs. (4) and (5) where $b_1(\lambda)$ is the slope of $\rho I(\rho)$, $b_0(\lambda)$ is the intercept of $\rho I(\rho)$, and c is a function of the amplitude of the incident light and the system response function. Because the measured intensities were referenced to a measurement of a diffuse reflector with a flat wavelength response, c does not depend on wavelength.

$$\mu_a(\lambda) = \frac{c b_1^2(\lambda)}{\exp[b_o(\lambda)]}, \tag{4}$$

$$\mu_s'(\lambda) = \frac{b_1^2(\lambda)}{3\mu_a(\lambda)} - \mu_a(\lambda). \tag{5}$$

We determined the constant c by measuring the elastic scatter signal as a function of fiber separation in 10% whole milk or suspensions of polystyrene spheres with and without the addition of a solution of red food coloring with a known absorption coefficient. The change in absorbance can then be used to evaluate c.

The experimentally determined values for μ_s' for suspensions of polystyrene spheres are compared with calculations of μ_s' in Fig. 7. The efficiency factors Q_s, Q_a and the distribution of scattering angles $P(\theta)$ were calculated for each size of sphere with a value of 1.59 used for the index of the polystyrene spheres and a value of 1.33 for the index of the suspending medium. The reduced scattering coefficient μ_s' was then determined according to Eq. (2). Calculations for both spheres of uniform dimension and for a mixture of discrete sphere sizes are shown in Fig. 7. The curves have been scaled such that the area under the theoretical curves is equal to the area under the corresponding experimental curves. The wavelength dependencies of the theoretical and experimental curves are quite close. The theoretical curve of μ_s', calculated for a single sphere size, oscillates as a function of wavelength. The result of our

summing the contributions of several sizes of spheres is that this oscillation is damped out.

In the derivation of Eqs. (4) and (5) the wavelength dependence of the speed of light in the medium that is due to the dispersion of the medium has been ignored. This is a reasonable approximation. Based on measurements of the dispersion of water, v is expected to change by $<0.8\%$ over the wavelength range 400-700 nm. Therefore, the wavelength dependence of c that is due to this effect is very weak. Wavelength-dependent errors in c may also be due to differences in dispersion of air and the medium being measured. The system response function is determined with the fibers in air above a piece of diffuse reflecting material; however, the measurements were performed with the fibers in an aqueous medium. The reflectance of photons at the fiber interface is a function of the indices of refraction of the fiber and the medium it is in contact with. Because air and water have different dispersions, measurement of the system response with an air-to-fiber instead of a water-to-fiber interface causes small wavelength-dependent errors in c. These errors are $<1\%$ for aqueous media.

B. Measurements at Large Source Detector Separations

The experimental system was comprised of a xenon arc lamp (Optical Radiation Corporation compact lamp, Azusa, Calif.), optical fibers for light delivery to and collection from the tissue phantom, a spectrograph and a thermoelectrically cooled CCD detector [Fig. 6(a)]. The fiber-optic probe consisted of several collection fibers arranged linearly from the source fiber. The bottom surface of the probe had dimensions of 4.5 cm $\times$ 3 cm and was painted flat black. Ten fibers could be imaged simultaneously onto the CCD array. The relative efficiency of light collection by each fiber was determined with the use of an integrating sphere and a separate light-delivery fiber. We determined the entire optical system response for a subsystem containing only one collection fiber by replacing the tissue phantom with a diffuse reflecting material, such as Spectralon, that has a flat response as a function of wavelength. By combining the optical system response function measured using one collection fiber, and the measurement of the relative light collection efficiency of the collection fibers, we measured the light intensity as a function of distance from the collection fibers to within a constant.

The phantom consisted of 15% Intralipid-10% in a roughly cylindrical container with a diameter and height of 30 cm and 9 cm, respectively. Small amounts of red food coloring were added. The Intralipid still appeared white after the addition of the food coloring. The absorbance of the red food coloring solution was also measured on a Cary spectrophotometer. We made wavelength-dependent measurements of scattered light at delivery-collection fiber center-to-center separations of 1.62, 1.8, 2.0, 2.2, and 2.4 cm by placing the optical probe on the surface of the medium. The light-delivery fiber was 1000 μm in diameter and the collection fibers were 400 μm, although they were coupled into a harness of fibers that were 200 μm in diameter. The numerical aperture of the fibers was 0.22. The integration time for measurement of the Intralipid was 4 s.

The light intensity as a function of distance ρ from the delivery fiber was modeled with an expression given below that is similar to that of Farrell *et al.*[25] The mismatch in boundary conditions was assumed to be small, and A was 1.06 for all of the fits. As pointed out by Haskell *et al.*, this expression neglects the fluence rate term.[26] For the parameters used here, this term is negligible. Nonlinear fits of light intensity as a function of fiber separation were performed. The three parameters of the fits were $\mu_t'(\lambda)$, $\mu_{\text{eff}}(\lambda)$, and the overall amplitude factor, I_0. At the distances measured, the shape of these curves can be used to determine $\mu_{\text{eff}}(\lambda)$. However, different pairs of $\mu_a(\lambda)$ and $\mu_s'(\lambda)$ with the same values of μ_{eff} do not result in differently shaped curves. The amplitude, in contrast, does change. Therefore, to determine $\mu_s'(\lambda)$ and $\mu_a(\lambda)$, it is necessary to determine I_0. Because both the response of a single delivery-collection pair of fibers to Spectralon was measured and because the relative response of all of the collection fibers was measured, it was possible to treat the data so that I_0 was not a function of wavelength. To determine I_0, the intensity as a function of fiber separation and wavelength was fit iteratively with different values of I_0. When the correct value of I_0 was reached, the difference in absorbance between measurements made with different amounts of red dye present agreed with the predictions based on the spectrophotometer measurements.

$$I(\rho) = I_0\left[\frac{1}{\mu_t'}\left(\mu_{\text{eff}} + \frac{1}{r_1}\right)\frac{\exp(-\mu_{\text{eff}} r_1)}{r_1^2} + \left(\frac{1}{\mu_t'} + 2z_b\right)\left(\mu_{\text{eff}} + \frac{1}{r_2}\right)\frac{\exp(-\mu_{\text{eff}} r_2)}{r_1^2}\right], \tag{6}$$

where

$$r_1 = \left[\left(\frac{1}{\mu_t'}\right)^2 + \rho^2\right]^{1/2}, \quad r_2 = \left[\left(\frac{1}{\mu_t'} + 2z_b\right)^2 2 + \rho^2\right]^{1/2},$$

$$\mu_{\text{eff}} = \sqrt{\frac{\mu_a}{D}}, \ \mu_t' = \mu_a + \mu_s' \text{ and } z_b = 2AD,$$

where $D = (1/3\mu_t')$ and A is related to the internal reflection.

The absorber was added to Intralipid in small increments. Figure 8 shows the change in absorbance that is due to the incremental addition of the red dye and the expected change in absorbance based on measurements of the solution of the red food coloring made in a standard spectrophotometer. As pointed out above, I_0 was chosen to make these curves agree in amplitude. The shift in the peak of the absorbance has also been seen in measurements with milk used as the scattering medium and is consistent with

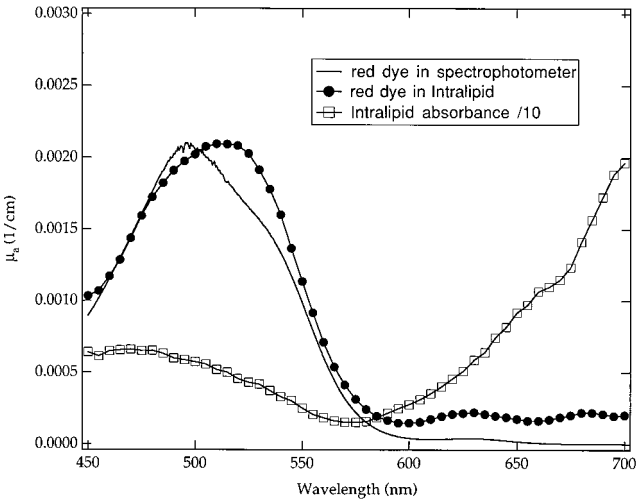

Fig. 8. Comparison of the measured change in absorbance that is due to the addition of a tiny amount of red food coloring to the expected change based on spectrophotometer measurements of a solution of red food coloring. The open squares measured absorbance of 15% Intralipid-10% divided by a factor of 10.

a change in the shape of the absorbance of the red food coloring with concentrations that we measured. By subtracting the measured absorbance of the red dye from the total absorbance of the solution of Intralipid and dye, we can calculate the absorbance of the 15% Intralipid-10%, which is shown in Fig. 8 (divided by 10). From 450 to almost 600 nm, the absorbance is similar in shape to that measured by Flock *et al.*,[27] although it is slightly higher in amplitude. The increase in absorbance above 600 nm, however, contradicts their results.

The measured reduced scattering coefficient of 15% Intralipid-10% is shown in Fig. 9. The absolute value is higher than the average, but still in the range

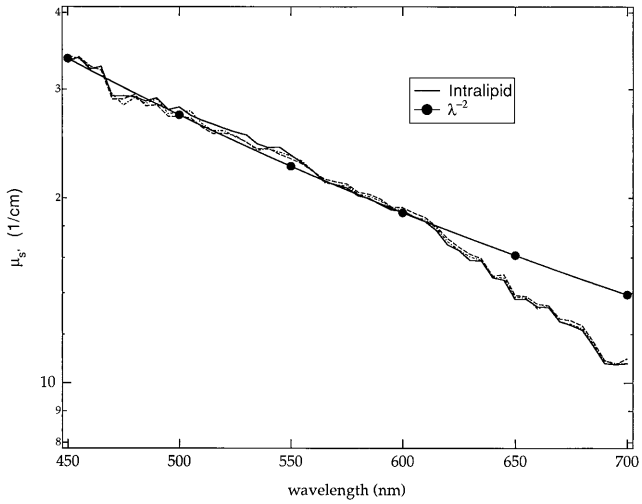

Fig. 9. Measured reduced scattering coefficient of Intralipid. This was performed for three different Intralipid suspensions with varying amounts of red food coloring added (the maximum absorption of the red food coloring varied from 0.009 to 0.013 cm^{-1}). The curves (which are all in the figure) are almost indistinguishable.

of literature values reported by Flock *et al.*[27] The wavelength dependence of the reduced scattering coefficient can be used to estimate the average size of the scattering particles. From 450 to 600 nm, the wavelength dependence of the $\mu_s'(\lambda)$ is expressed accurately by λ^{-2}. A comparison with Fig. 4 finds that the scattering particles are of the order of 75 nm in radius. The average radius of particles in Intralipid was found to be 46.5 nm by van Staveren *et al.* using transmission electron microscopy.[28]

C. Measurements with Small Fiber Separations: Sensitivity to Particle Size

In this subsection we demonstrate that sensitivity to structural features of the scatterers can be varied by changing the separation d between light delivery and collection fibers. For small values of d ($d < 1/\mu_s'$), measurements are more sensitive to sphere size than for large values of d ($d > 1/\mu_s'$).

Aqueous solutions of 0.2485-, 0.483-, and 1.5-μm-radius polystyrene spheres were measured with fiber separations of 0.05 and 1.649 cm. The concentrations of the spheres by weight were, respectively, 0.119%, 0.154%, and 0.34%. The reduced scattering coefficients were 4.64, 4.85, and 1.53 cm^{-1}, respectively, at 600 nm. A 600-μm delivery fiber (0.48 NA) and a 400-μm collection fiber (0.22 NA) were used. The fibers penetrated the surface of the suspension less than 1 mm. Sample volumes greater than 30 mL were measured in black-walled cylinders with diameters of ~3.5 cm.

The collected elastic scatter signal I is shown in Fig. 10. The curves have been normalized to a value of 1 at 500 nm. The three curves at a fiber center-to-center separation of 500 μm are quite distinctive. The oscillations seen in the elastic scatter signal of the 1.5-μm spheres are not an artifact. Similar oscillations for 1.85-μm-radius spheres have been seen in Monte Carlo simulations that employ Mie theory.[29] At a source-to-detector separation of 1.649 cm, the wavelength dependence of the elastic scatter signal of the three sizes of spheres are all similar.

4. Discussion and Conclusions

The main conclusions from Section 2 are: (1) Small changes in size and index of refraction cause greater changes in the wavelength dependence of $P(\theta, \lambda)$ and $\mu_s(\lambda)$ than in $\mu_s'(\lambda)$ for scatterers relevant to tissue. (2) Measurements in geometries where high-angle scattering is enhanced are expected to be more useful for the differentiation of morphological features. (3) As particle size increases from the Rayleigh regime to a regime in which $r \geq \lambda$ but $x < 70$, the wavelength dependence of $\mu_s'(\lambda)$, which is approximately a monotonically decreasing function of wavelength, changes from λ^{-4} to $\lambda^{-0.37}$. For relative refractive indices typical of tissue, this wavelength dependence does not change with refractive index, but rather depends only on particle size.

In Subsection 3.C, we demonstrated that measurements made with small source detector separations are more sensitive to the size of the

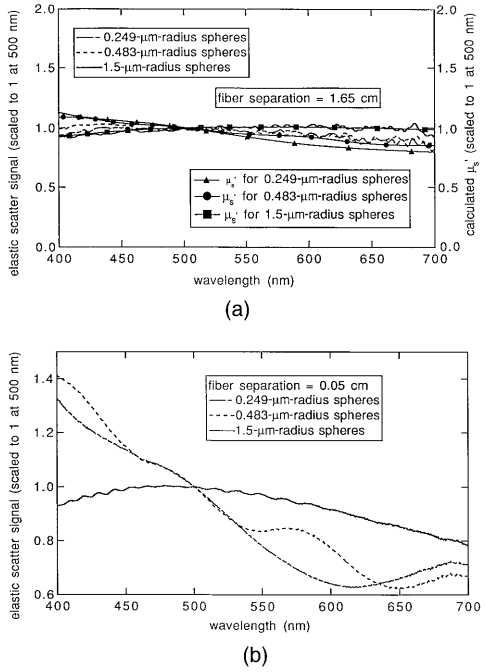

Fig. 10. (a) Elastic measurements on three suspensions of different size polystyrene spheres with source-to-detection fiber separation of 1.65 cm. (b) Elastic measurements on three suspensions of different size polystyrene spheres with source-to-detection fiber separation of 0.05 cm. All curves have been scaled to have a value of 1 at 500 nm.

scatterers than measurements made with large source detector separations. This is consistent with the results of Section 2 that show that μ_s and $P(\theta)$ are more sensitive to the size and shape of the scatterer than is μ_s'. Because measurements at the larger fiber separations are the result of many scattering events, the reduced scattering coefficient μ_s' is the only parameter needed to describe the scattering. At the smaller fiber separations, commensurate with application of a fiber probe through an endoscope, scattering is a more complicated function of μ_s and $P(\theta)$. In addition, scattering measurements with small fiber separations are expected to enhance sensitivity to high-angle scatter. This is because photons must turn around by way of high-angle scattering events to be detected. As discussed in Section 2, this also aids in the assessment of tissue morphology.

Measurements at large source-to-detector separations can yield values for the reduced scattering coefficient and the absorption coefficient. Broad wavelength measurements at six fiber separations from 1.6 to 2.4 cm were made in 4 s on a suspension of Intralipid and dye. The results of these measurements yielded reduced scattering and absorption coefficients consistent with those found in the literature. The wavelength dependence of the reduced scattering coefficient was used to estimate the size of the scattering particles in the Intralipid. The value of ~75 nm that we obtained agrees well with an average size of 47 nm. Broad wavelength, cw measurements of μ_s' for three suspensions of polystyrene microspheres were also made with a less accurate experimental system. There was good agreement between the experiment and calculations with Mie theory used for the prediction of the wavelength dependence of μ_s'. However, agreement between measured and predicted values of the magnitude of μ_s' was less accurate and differed by approximately a factor of 2. This illustrates an important point. The measurement of the absolute values of μ_s' is more difficult than the measurement of the wavelength dependence. Therefore techniques for understanding optical properties based on the wavelength dependence rather than the absolute value of μ_s' are important.

Other groups have also begun investigating the use of cw and or white light systems for measuring μ_s' and μ_a. Chance *et al.* have also demonstrated the use of a cw system for measuring μ_s' and μ_a.[30] Their method differed from ours in that the calibration used was a turbid medium for which both μ_a and μ_s' were known, whereas our calibrations required only knowledge of μ_a. Liu *et al.* have also made measurements of optical properties and introduced an approximation to the Farrell expression.[31] Recently, measurements of light intensity as a function of distance from the source and of $\mu_a(\lambda)$ and $\mu_s'(\lambda)$ with the use of an experimental system similar to the one used to make the measurements of Intralipid have been reported.[32,33]

Throughout this paper we have approximated the scatterers in tissue as homogeneous spheres, and we used Mie theory to predict scattering characteristics. Many of the expected scatterers in tissue are not homogenous and are not spherical. Therefore the question arises as to the range of validity of this approximation. Comparison of experiment and theory in measurements of red blood cells and yeast cells partially answers this question. Measurements of μ_s and μ_s' have been compared to Mie theory calculations for red blood cells.[34] Deviations in μ_s typically were less than 10%, but differences in measured and predicted values of g caused larger (factor of 2) discrepancies in μ_s'. Nonetheless, trends that were seen in the experimental data (as a function of osmollality or RBC species) were also seen in the Mie calculations. Measurements of μ_s' of yeast cells have also been compared with Mie calculations of μ_s'.[35] By varying the cell refractive index, good agreement was found for a variety of yeast cells. Therefore, we believe that the trends we report in this paper are relevant to scattering from real cells in tissue.

We have demonstrated that measurements of μ_a and μ_s' can be made rapidly with a cw, white light system and that these measurements are sensitive to changes in absorbance of ~0.001 cm^{-1}. We have also shown that the wavelength dependence of $\mu_s'(\lambda)$ can be used to estimate the size of the scatterers in Intralipid. Possible applications for this technique are monitoring real-time changes of multiple, physiologically important chromophores *in vivo*. The sys-

tem can also be used to characterize cell suspensions. An interesting question that can be answered by such a measurement is: What are the sizes of the scatterers that dominate the scattering in cells? We will address this question in a future paper.

The authors gratefully acknowledge the help and support of JoAnne Lacey and Heather Miller in some of the experiments described in this paper as well as some preliminary work by Cynthia Broh. This research was funded primarily through the Laboratory Directed Research and Development program at Los Alamos National Laboratory, with additional support from the Historically Black Colleges and University program of the U.S. Department of Energy. We thank Ed Hull and Tom Foster for some very useful comments.

References and Notes

1. J. Wu, M. S. Feld, and R. P. Rava, "Analytic model for extracting intrinsic fluorescence in turbid media," Appl. Opt. **32,** 3585–3595 (1993).
2. E. M. Sevick and C. L. Burch, "Origin of phosphorescence signals reemitted from tissues," Opt. Lett. **19,** 1928–1930 (1994).
3. J. B. Fishkin, P. T. C. So, A. E. Cerussi, S. Fantini, M. A. Franceschini, and E. Gratton, "Frequency-domain method for measuring spectral properties in multiple-scattering media: methemoglobin absorption spectrum in a tissuelike phantom," Appl. Opt. **34,** 1143–1155 (1995).
4. M. S. Patterson, S. Andersson-Engels, B. C. Wilson, and E. K. Osei, "Absorption spectroscopy in tissue-simulating materials: a theoretical and experimental study of photon paths," Appl. Opt. **34,** 22–30 (1995).
5. S. A. Ahmed, Z.-W. Zang, K. M. Yoo, and R. R. Alfano, "Effect of multiple light scattering and self-absorption on the fluorescence and excitation spectra of dyes in random media," Appl. Opt. **33,** 2746–2750 (1994).
6. R. Bays, G. Wagnieres, D. Robert, D. Braichotte, J.-F. Savary, P. Monnier, and H. van den Bergh, "Clinical determination of tissue optical properties by endoscopically resolved reflectometry," Appl. Opt. **35,** 1756–1766 (1996).
7. S. Fantini, M. A. Franceschini, J. B. Fishkin, B. Barbieri, and E. Gratton, "Quantitative determination of chromophores in a strongly scattering media: a light-emitting-diode based technique," Appl. Opt. **33,** 5204–5213 (1994).
8. J. R. Mourant, I. J. Bigio, J. Boyer, R. L. Conn, T. Johnson, and T. Shimada, "Spectroscopic diagnosis of bladder cancer with elastic light scattering," Lasers Surg. Med. **17,** 350–357 (1995).
9. T. Vo-Dinh, M. Panjehpour, B. F. Overholt, C. Farris, F. P. Buckley III, and R. Sneed, "In vivo cancer diagnosis of the esophagus using differential normalized fluorescence (DNF) indices," Lasers Surg. Med. **16,** 41–47 (1995).
10. K. T. Schomacker, J. K. Frisoli, C. C. Compton, T. J. Flotte, J. M. Richter, N. S. Nishioka, and T. M. Deutsch, "Ultraviolet laser-induced fluorescence of colonic tissue: basic biology and diagnostic potential," Lasers Surg. Med. **12,** 63–78 (1992).
11. N. Ramanujan, M. F. Mitchell, S. Warren, S. Thomsen, E. Silva, and R. Richards-Kortum, "*In vivo* diagnosis of cervical intraepithelial neoplasia using 337-nm-excited laser-induced fluorescence," Proc. Nat. Acad. Sci. U.S.A. **91**(21), 10193–10197 (1994).
12. The spheres are actually a mixture of polystyrene, polystyrene divingl-benzene, polyvinyltoluene, and/or butadiene.
13. G. C. Salzman, "Light scattering analysis of single cells," in *Cell Analysis*, N. Catsimpoolas, ed. (Plenum, New York, 1982), Vol. 1, pp. 111–143.
14. C. Lenter, ed., *Geigy Scientific Tables* (Ciba-Geigy, Basle, 1984), Vol. 3, p. 69.
15. A. Brunsting and P. F. Mullaney, "Differential light scattering from spherical mammalian cells," Biophys J. **14,** 439–453 (1974).
16. R. C. Weast, ed., *CRC Handbook of Chemistry and Physics* (CRC Press, Boca Raton, Fla., 1984), p. D-221.
17. S. Fujime, M. Takasaki-Oshito, and S. Miyamoto, "Dynamic light scattering from polydisperse suspensions of large spheres," Biophys. J. **54,** 1179–1184 (1988).
18. This is the definition of the size parameter used by Bohren and Huffman (Ref. 19, p. 100). The definition $x = 2\pi r/\lambda$ is also found frequently in the literature.
19. C. F. Bohren and D. R. Huffman, *Absorption and Scattering of Light by Small Particles* (Wiley, New York, 1983).
20. R. A. Meyer, "Light scattering from biological cells: dependence of backscatter radiation on membrane thickness and refractive index," Appl. Opt. **18,** 585–588 (1979).
21. M. Kerker, D. D. Cooke, H. Chew, and P. J. McNulty, "Light scattering by structured spheres," J. Opt. Soc. Am. **68,** 592–601 (1978).
22. R. Graaff, J. G. Aarnoose, J. R. Zijp, P. M. A. Sloot, F. F. M. de Mul, J. Greve, and M. H. Koelink, "Reduced light-scattering properties for mixtures of spherical particles: a simple approximation derived from Mie calculations," Appl. Opt. **31,** 1370–1376 (1992).
23. J. B. Fishkin and E. Gratton, "Propagation of photon-density waves in strongly scattering media containing an absorbing semi-infinite plane bounded by a straight edge," J. Opt. Soc. Am. A **10,** 127–140 (1993).
24. B. J. Tromberg, L. O. Svaasand, T.-T. Tsay, and R. C. Haskell, "Properties of photon density waves in multiple-scattering media," Appl. Opt. **32,** 607–616 (1993).
25. T. J. Farrell, M. S. Patterson, and B. Wilson, "A diffusion theory model of spatially resolved, steady-state diffuse reflectance for the noninvasive determination of tissue optical properties *in vivo*," Med. Phys. **19,** 879–888 (1992).
26. R. C. Haskell, L. O. Svaasand, T-C. Feng, M. S. McAdams, and B. Tromberg, "Boundary conditions for the diffusion equation in radiative transfer," J. Opt. Soc. Am. A **11,** 2727–2741 (1994).
27. S. T. Flock, S. L. Jacques, B. C. Wilson, W. M. Star, and M. J. C. van Gemert, "Optical properties of intralipid: a phantom medium for light propagation studies," Lasers Surg. Med. **12,** 510–519 (1992).
28. H. J. van Staveren, C. J. Moes, J. van Marle, S. A. Prahl, and M. J. C. van Gemert, "Light scattering in Intralipid-10% in the wavelength range 400–1100 nm," Appl. Opt. **30,** 4507–4514 (1991).
29. J. Boyer, J. R. Mourant, and I. J. Bigio, "Theoretical and experimental investigations of elastic scattering spectroscopy as a potential diagnostic for tissue pathologies," in *Advances in Optical Imaging and Photon Migration*, R. R. Alfano, ed., Vol. 21 of 1994 OSA Proceedings (Optical Society of America, Washington, D.C., 1994), pp. 265–268.
30. B. Chance, H. Liu, T. Kitai, and Y. Zhang, "Effects of solutes on optical properties of biological materials: models, cells and tissue," Anal. Biochem. **227,** 351–362 (1995).
31. H. L. Liu, D. A. Boas, Y. T. Zhang, and A. G. Yodh, "Determination of optical properties and blood oxygenation in tissue using continuous NIR light," Phys. Med. Biol. **40,** 1983–1993 (1995).
32. J. R. Mourant, A. H. Hielscher, H. D. Miller, and J. S. George, "Broadband monitoring of physiological changes with a continuous light tissue spectrometer," in *Biomedical Optical Spectroscopy and Diagnostics*, Vol. 3 of Trends in Optics and Photonics (Optical Society of America, Washington, D.C., 1996), Vol. 3, pp. 37–42.

33. M. G. Nichols, E. L. Hull, and T. H. Foster, "Spatially and spectrally resolved steady-state diffuse reflectance measurements of the optical properties of tissue-simulating phantoms," in *Biomedical Optical Spectroscopy and Diagnostics*, Vol. 3 of Trends in Optics and Photonics (Optical Society of America, Washington, D.C., 1996), Vol. 3, pp. 50–58.
34. J. M. Steinke and A. P. Shepherd, "Comparison of Mie theory and the light scattering of red blood cells," Appl. Opt. **27,** 4027–4033 (1988).
35. B. Beauvoit, H. Liu, K. Kang, P. D. Kaplan, M. Miwa, and B. Chance, "Characterization of absorption and scattering properties of various yeast strains by time-resolved spectroscopy," Cell Biophys. **23,** 91–109 (1993).